Endothelial Protective Monocyte Patrolling in Large Arteries Intensified by Western Diet and Atherosclerosis

Amado Quintar[1,2], Sara McArdle[1], Dennis Wolf[1], Alex Marki[1], Erik Ehinger[1], Melanie Vassallo[1], Jacqueline Miller[1], Zbigniew Mikulski[1], Klaus Ley[1]§, Konrad Buscher[1]§

[1]La Jolla Institute for Allergy and Immunology, Division of Inflammation Biology, La Jolla, California, USA; [2]Centro de Microscopia Electronica, INICSA-CONICET, Facultad de Ciencias Medicas, Universidad Nacional de Cordoba, Cordoba, Argentina.

§ shared senior authorship

***Running title*:** Monocyte Patrolling in Arteries

Subject Terms:
Inflammation
Atherosclerosis
Vascular Disease

Address correspondence to:
Dr. Konrad Buscher
Division of Inflammation Biology
La Jolla Institute for Allergy & Immunology
9420 Athena Circle Drive
La Jolla, CA 92037
Tel: (858) 752 6661
konrad@lji.org

Dr. Klaus Ley
Division of Inflammation Biology
La Jolla Institute for Allergy & Immunology
9420 Athena Circle Drive
La Jolla, CA 92037
Tel: (858) 752 6661
klaus@lji.org

In February 2016, the average time from submission to first decision for all original research papers submitted to *Circulation Research* was 15.4 days

ABSTRACT

***Rationale*:** Non-classical mouse monocyte (CX3CR1^{high}, Ly-6C^{low}) patrolling along the vessels of the microcirculation is critical for endothelial homeostasis and inflammation. Due to technical challenges it is currently not established how patrolling occurs in large arteries.

***Objective*:** This study was undertaken to elucidate the molecular, migratory and functional phenotype of patrolling monocytes in the high shear and pulsatile environment of large arteries in healthy, hyperlipidemic and atherosclerotic conditions.

***Methods and Results*:** Applying a new method for stable, long-term two-photon intravital microscopy of unrestrained large arteries in live CX3CR1-GFP mice, we show that non-classical monocytes patrol inside healthy carotid arteries at a velocity of 36 μm/min, three times faster than in microvessels. The tracks are less straight but lead preferentially downstream. The number of patrolling monocytes is increased 9-fold by feeding wildtype mice a western diet or by applying topical TLR7/8 agonists. A similar increase is seen in CX3CR1$^{+/GFP}$/apoE$^{-/-}$ mice on chow diet, with a further 2-3-fold increase on western diet (22-fold over healthy). In plaque conditions, monocytes are readily captured onto the endothelium from free flow. Stable patrolling is unaffected in CX3CR1-deficient mice and involves the contribution of LFA-1 and α_4 integrins. The endothelial damage in atherosclerotic carotid arteries was assessed by electron microscopy and correlates with the number of intraluminal patrollers. Abolishing patrolling monocytes in Nr4a1$^{-/-}$ apoE$^{-/-}$ mice leads to pronounced endothelial apoptosis.

***Conclusions*:** Arterial patrolling is a prominent new feature of non-classical monocytes with unique molecular and kinetic properties. It is highly upregulated in hyperlipidemia and atherosclerosis in an CX3CR1-independent fashion, and plays a potential role in endothelial protection.

Keywords:
Patrolling monocyte, atherosclerosis, endothelium, western diet, imaging, inflammation, plaque

Nonstandard Abbreviations and Acronyms:

ILTIS	intravital live cell triggered imaging system
WD	western diet

INTRODUCTION

Intravascular interactions with the endothelium under shear conditions are a crucial feature of homeostatic and inflammatory immune cells to sense and react to local stimuli [1]. Such interactions include rolling, crawling and patrolling, where patrolling is defined as long-distance, persistent migratory movement on the apical aspect of endothelial cells with and against the direction of flow and without immediate extravasation [2]. Patrolling was discovered in the microcirculation [2], and all reports of patrolling to-date concern microvessels in various organs [3–5]. While capillaries and postcapillary venules can be readily imaged in vivo, arterial imaging poses technical difficulties and, as a consequence, little is known about leukocyte-endothelial interactions in large arteries *in situ*. Patrolling in large arteries has not been described.

Cells of the monocytic lineage show a vast repertoire of functions, and two individual subsets are characterized in detail. Classical (Ly-6C^{high} CX3CR1^{low}, CCR2^{high}) monocytes are highly responsive to inflammatory signals, invade inflamed tissues early, and can differentiate into macrophages [6]. In contrast, non-classical monocytes (Ly-6C^{low}, CX3CR1^{high}, CCR2^{low}) exert endothelial surveillance by endovascular slow patrolling in search of tissue cues [2,7]. Mean patrolling velocity in the microcirculation is 12 (4-20) μm/min [2]. Motion patterns include waves, hairpins, and loops, with a confinement ratio (distance traveled divided by path length) of about 0.5 in venules [2]. Active patrolling depends on the $\alpha_L\beta_2$-integrin (LFA-1) [2]. Local TLR7 dependent endothelial and tissue signals activate patrolling monocytes on the endothelium in an CX3CR1-dependent manner for scavenging of debris in collaboration with neutrophils [3,8]. Ly-6C^{high} monocytes are blood-borne precursors of patrollers [9], and the transcription factor Nr4a1 controls the development and survival in the bone marrow [10]. Recently, it has been reported that the pulmonal microcirculation harbors a high amount of patrollers that are crucial in preventing pulmonal metastasis [4].

In atherosclerosis, monocytes have gained long standing attention as precursors of plaque phagocytes [11,12]. Both local macrophage proliferation [13] and steady recruitment of blood-borne monocytes (mostly Ly-6C^{high}) to plaque regions contribute to disease progression [14–16]. A hyperlipidemia-associated monocytosis is mostly fueled by classical monocytes [17], but elevated non-classical monocytes have also been reported [18]. The chemokine receptors CCR1 and CCR5 are thought to be involved in classical monocyte entry into atherosclerotic lesions [16,18], where they can differentiate into CD11b$^+$CD11c$^+$ plaque macrophages and tip-DCs with a pro-inflammatory phenotype [11]. Nr4a1 knockout mice lack non-classical monocytes, show no patrolling in the microcirculation, and exhibit exacerbated atherosclerosis [3,19,20]. The latter finding is attributed to hyperinflammatory plaque macrophages [20]. The temporo-spatial fate of non-classical monocytes in atherosclerosis remains unclear.

We recently developed an intravital live cell triggered imaging system (ILTIS) that allows stable *in situ* two-photon microscopy imaging of unrestrained carotid arteries with intact adventitia [21]. Here, using ILTIS, we investigate the molecular and kinetic features of arterial monocyte patrolling in healthy, hyperlipidemic, and atherosclerotic conditions. We show that patrolling occurs under homeostatic conditions, is highly upregulated at early and late stages of atherogenesis, and potentially protects from endothelial apoptosis.

METHODS

Animals.

CX3CR1-GFP reporter mice were provided by S. Jung (Weizmann Institute, Israel) and back-crossed onto C57BL/6J until a genetic purity of > 99% was achieved (SNP analysis by Dartmouse, Dartmouth College, USA). ApoE$^{-/-}$ mice were obtained from Jackson Laboratory (stock number: 002052). CX3CR1-GFP and apoE$^{-/-}$ mice were crossed, resulting in CX3CR1$^{+/GFP}$ apoE$^{-/-}$ mice [21]. Homogenous expression of CX3CR1-GFP leads to a functional protein knockout [22]. In experiments comparing CX3CR1$^{+/GFP}$ and CX3CR1$^{GFP/GFP}$ genotypes, littermates were used. Nr4a1$^{-/-}$ apoE$^{-/-}$ mice were previously described [20]. All animal experiments were approved by the local animal ethics committee.

Intravital live cell triggered imaging system (ILTIS).

Technical details of the ILTIS setup have been described before [21]. Preparation of the large arteries was done carefully with minimal handling to prevent surgery-related inflammation. The adventitia was not removed. Tissue was kept moist with phophate-buffered saline at 35-37°C. All imaging experiments were conducted on a Leica SP5 system using a water-dipping objective (Olympus XLUMPLFL 20X NA 0.95) and an objective heater. The system is composed of a DM6000 microscope, a Ti-Sapphire laser (Chameleon Ultra II, Coherent), tuned to 920 nm, a resonant scan head for fast scanning, and a Leica trigger box. Three NDD detectors were used in most of the experiments with the following filter sets: 460/40 for second harmonics, 513/50 for GFP, and 640/40 for texas red. Videos were recorded in 512 x 256 pixel resolution (= 455 x 227 μm) for 30 – 90 minutes. Under ketamine/xylazine anesthesia, the heart rate was typically at about 300 – 400 bpm. An Arduino-based circuit allowed image acquisition in triplets triggered by the signal of the pulse oxymeter attached to the thigh.

Cell tracking and data analysis.

After ILTIS post-processing, which included frame selection and 2D registration using self-made plugins in ImageJ [21], a final frame rate of 1 – 1.5 frames/s was achieved. In all movies analyzed, patrolling GFP+ cells were detected using an absolute intensity threshold, and tracked using Imaris' autoregressive motion algorithm (Bitplane). Only tracks with a duration longer than 90 sec were considered patrolling cells. To de-noise residual motion artifacts of imaging, cell tracks were smoothed using Matlab as described previously [21]. For quantification, patrolling monocytes were tracked for 17 min in each movie unless indicated otherwise. Fast cells moving at over 100 μm/min were considered rolling.

Further details are denoted in supplemental materials.

RESULTS

Non-classical monocytes patrol healthy arteries.

We used heterozygous CX3CR1$^{+/GFP}$ reporter mice [22] for intravital imaging. In these mice, non-classical monocytes are brightly fluorescent while classical monocytes are dimly fluorescent (supplemental fig. I). We confirmed ex vivo that the GFP^{dim} monocytes are not detectable using ILTIS (supplemental fig. II). Macrophages in the vessel wall are also GFP^{high} (fig. 1a); therefore, we used a blood tracer to clearly identify intraluminal monocytes (fig. 1a). In healthy 8 week-old mice on chow diet, we observed CX3CR1-GFP^{high} patrollers along the distal part of the external carotid artery (fig. 1a,b). The patrolling velocity averaged about 36 μm/min (0.5 μm/s) with a low confinement ratio (straightness) (fig. 1c). Under these experimental conditions, most patrolling events lasted about 5 – 10 minutes until detachment (fig. 1c). To exclude a technical bias in measurements, we used the ILTIS technique on the ear microcirculation and obtained similar results to those previously published (table I) [2,3].

Arterial patrolling is induced by TLR7/8 agonists and requires $\alpha_L\beta_2$ and α_4 integrins.

It has been reported that the local TLR7/8 agonist R848 increases the number of patrolling monocytes in venules due to endothelial activation [3]. Topical application of R848 on the carotid artery in healthy 8 week old mice attracted CX3CR1-GFP^{high} patrollers in a time-dependent manner. Patrolling activity was increased over 2- and 10-fold after 3 and 5 hours incubation, respectively (fig. 2a,b). In contrast to the microcirculation [3], LFA-1 blockade by i.v. antibodies induced detachment of only about 50% of CX3CR1-GFP^{high} patrollers, as assessed by intravital microscopy (fig. 2c). Additional blocking of the VLA-4 integrin (α_4 blockade) abolished most patrolling (fig. 2c). While the directionality showed a flow bias (downstream) at baseline conditions, blocking LFA-1 or VLA-4 revealed a pan-directional patrolling pattern (fig. 2d). The net velocity decreased in response to R848 (fig. 2e). After LFA-1 and LFA-1/VLA-4 blockade, the motion characteristics of the remaining patrollers did not significantly change (fig. 2e). These results suggest that endothelial TLR-7/8-dependent signals effectively trigger patrolling in arteries in an LFA-1- and integrin α_4-dependent manner.

Increased patrolling in hyperlipidemia independent of CX3CR1.

Next, we investigated the impact of hyperlipidemia on patrolling activity. In CX3CR1$^{+/GFP}$ apoE$^{+/+}$ mice on western diet (WD) for 4 weeks, we observed an 9-fold increase in CX3CR1-GFP^{high} patrolling compared to baseline (fig. 3a, movie I). Comparably, in CX3CR1-GFP^{high} apoE$^{-/-}$ mice on chow diet (age 4 – 6 months) an 8-fold increase was detected (fig. 3a,b). Similar to R848 induction, patrolling could be blocked by LFA-1 and VLA-4 antibody inhibition (fig. 3c). Migration analysis over 45 min shows that some areas of the endothelium were preferentially frequented in the carotid artery (fig. 3d, movie II). The overall directionality of their endothelial migration was downstream (fig. 3e,f). Both models of hyperlipidemia showed no significant differences in patrolling microkinetics (fig. 3g).

Homozygous expression of CX3CR1-GFP leads to a functional protein knockout that allows to study monocyte behavior in CX3CR1-deficient conditions [2,22]. In these mice (CX3CR1$^{GFP/GFP}$ apoE$^{-/-}$ on chow diet), the number of patrolling monocytes and the migration pattern was similar to heterozygous CX3CR1$^{+/GFP}$ apoE$^{-/-}$ mice, suggesting that patrolling in large arteries occurs independently of CX3CR1 (supplemental fig. III).

Massive patrolling in atherosclerotic arteries.

In CX3CR1$^{+/GFP}$ apoE$^{-/-}$ mice fed WD for 6 weeks, arterial plaques were present in the carotid artery (fig. 4a,b) [21]. High and low GFP expression of non-classical and classical monocytes, respectively, was

confirmed in these mice using flow cytometry (supplemental fig. I). NK and T cell subsets are known to be GFP positive in CX3CR1-GFP mice [22]. Therefore, we tested whether GFP is an adequate marker to identify patrolling monocytes in arteries with active plaques. Atherosclerotic aortas including carotid arteries were explanted, flushed, and the flow through analyzed by flow cytometry. This experiment confirmed that the majority (about two thirds) of intraluminal GFP^{high} cells in atherosclerotic arteries are patrolling monocytes (supplemental fig. IV).

In these atherogenic conditions, we observed many GFP+ macrophages in the plaque (fig. 4a), whereas patrolling monocytes could be identified in the lumen in contact with the plasma tracer (fig. 4b). Of all interacting intravascular CX3CR1-GFP positive cells, about 60-70% were patrolling, and about 30% of these showed jerky patrolling with intermittent rolling (fig. 4c). We observed a strong increase in patrolling activity, about 22-fold over healthy conditions, and about 2-3-fold over $apoE^{-/-}$ on chow diet (fig. 4d). The patrolling phenotype differed between plaque-close and –distant areas. Patrolling monocytes in plaque proximity showed a lower velocity, longer duration and a lower confinement ratio (fig. 4e).

The time resolution of ILTIS is about 1 frame/second (after frame selection), which allows us to investigate kinetic events prior to and during patrolling. Many GFP+ cells attached to the endothelium from free flow (movies III, IV). Frame by frame analysis revealed that short rolling interactions often precede patrolling (fig. 5a,b). Intermittent "jumps" (short spikes in velocity, i.e. rolling) during patrolling were also evident (fig. 5a; movies III- IV).

Arterial patrolling is associated with endothelial damage.

We analyzed the endothelium of the carotid artery in hyperlipidemic and atherosclerotic conditions using transmission electron microscopy (TEM). Morphological signs of endothelial damage included loss of electrodensity, vacuolization (incipient signs), cytoplasmic edema, chromatin fragmentation, nuclear condensation, exnucleation, cell shedding and denudation (severe signs). The endothelial cell layer in control mice on chow diet was healthy (fig. 6a,b and suppl. fig V). Western diet and apoE-knockout increased the extent of damaged endothelial cells per section, and $apoE^{-/-}$ mice fed western diet showed a further increase (fig. 6a,b; supplemental fig. V). The extent of endothelial cell damage significantly correlated with the number of patrolling monocytes we observed in these conditions using ILTIS (fig. 6c), suggesting a response to local damage.

Nr4a1-deficient mice have been shown to lack most patrolling monocytes in the blood [10]. These mice on an $apoE^{-/-}$ background consuming western diet develop aggravated atherosclerosis [20]. We first asked whether patrolling monocytes are indeed depleted locally from the endothelium of atherosclerotic arteries. By flushing explanted aortas (fig. 7a), we confirmed fewer monocytes on the endothelium, and the remainders were classical monocytes (fig. 7b). In TEM analyses, the carotid endothelium of Nr4a1-deficient mice showed aggravated endothelial damage (more lesions per section) (fig. 7c,d; supplemental fig. V). Compared to $Nr4a1^{+/+}$ $apoE^{-/-}$ controls, the lesions preferentially comprised multiple severe signs of cell death. A TUNEL apoptosis assay confirmed a higher number of damaged endothelial cells in Nr4a1-deficient mice (supplemental fig. VI).

DISCUSSION

We show that patrolling monocytes monitor the endothelium of healthy carotid arteries. Net velocity of arterial crawling is about three times as fast as in the microcirculation (table I), and tracks preferentially lead downstream (with the blood flow), despite a low confinement ratio. Endothelial stimulation via TLR7/8 agonists, hyperlipidemia, and atherosclerosis triggers the accumulation of patrollers, with the latter condition having a 22-fold increase over baseline. Patrollers are readily captured from free flow, show short- and long-term interactions, and can alternate patrolling with rolling. Sequential blocking of LFA-1/VLA-4, but not VLA-4 alone, triggers detachment of arterial patrollers. The number of patrolling monocytes in situ correlates with the local endothelial damage, and patroller-deficient Nr4a1$^{-/-}$ mice show increased signs of endothelial cell death. These data establish the concept of arterial Ly-6C^{low} monocyte patrolling, lay out the fundamental migratory and molecular phenotype, and suggest an endothelial-protective role.

An elegant study by Chèvre et al. provided insight into neutrophil interactions in atherosclerotic carotid arteries by applying mechanial stabilization of the vessel [23]. In our study, a minimum video acquisition time of about 20 min or more was necessary to effectively describe slow monocyte patrolling. As vascular mechanical forces including pulsatile flow have been shown to impact on cellular responses [24,25], long term acquisition data with mechanical stabilization could be flawed. ILTIS microscopy does not require any physical contact with the artery during preparation or imaging [21]. Therefore, this technique is ideally suited for the purpose of this study.

Wall shear stress is low in venules, intermediate in large arteries, and high in small pre-capillary arterioles [25]. Unlike patrolling in arterioles and venules of the mesentery and dermis [2,3], we find a higher velocity, a lower confinement ratio, and no typical hairpin and loop-patterns in the carotid artery. It has been shown that T effector cells tend to crawl upstream (against the flow) under high shear conditions [26]. In contrast, the overall directionality of patrollers in the carotid artery was downstream (with the blood flow). This excludes the possibility of retrograde migration from the microcirculation. We observed a significant number of blood-borne monocytes attaching from free flow in atherosclerotic conditions. This was often preceded or interrupted by a short rolling step which suggests a cascade-like fashion of endothelial interactions in order to slow down the cell in medium/high shear conditions.

ApoE-knockout mice on chow or western diet develop an 8- or 22-fold increase in serum levels of VLDL/IDL, respectively, when compared to control mice [27]. It has been reported that elevated lipids such as βVLDL and LDL promote adhesion of monocytes to the endothelium [28–30]. Endothelial activation occurs early in atherosclerosis [24], and metabolite-related endogenous danger signals precede monocyte infiltration [31]. Our intravital imaging data confirms early non-classical monocyte accumulation in the carotid artery in mild hyperlipidemia. We also show that the TLR7 agonist R848 locally attracts patrolling monocytes, pointing to a conserved pathway in large arteries and the microcirculation [3]. A previous study suggested that TLR7 inactivation results in aggravated atherosclerosis [32]. Therefore, it could be hypothesized that TLR7 activation in damaged endothelium during atherogenesis is required to mount a protective response by patrolling monocytes.

In the microcirculation, R848-mediated accumulation of patrolling monocytes is CX3CR1-dependent. Notably, few patrollers also remained in CX3CR1-deficient mice. In contrast, massive patrolling in atherosclerosis is independent of CX3CR1, suggesting that the CX3CR1-independent fraction expanded. We found a requirement of the integrins LFA-1 ($\alpha_L\beta_2$) and VLA-4 ($\alpha_4\beta_1$). While only LFA-1 is relevant in microcirculatory patrolling [2,3], VLA-4 was recently implicated in patrolling of renal glomeruli [5]. Furthermore, as shown in both R848-triggered and hyperlipidemic conditions, about 50% of patrollers detach upon LFA-1 blockade alone, but many patrollers also require the sequential blockade of α_4 integrins to detach. This finding raises two main questions: First, do two CX3CR1-independent subsets of patrollers

exist in atherosclerosis, where one is strictly LFA-1-dependent and another one can also patrol via α_4 integrins? Second, how do changes of the atherosclerotic endothelium such as VCAM-1 upregulation [33,34] affect patroller recruitment? In this line, our data show that the plaque shoulder mediates different patrolling kinetics compared to plaque-distant sites. Interestingly, similar motion characteristics were found in R848 treated arteries, i.e. very low confinement ratios and velocities (table II). Finally, it also needs to be considered that we found around one third of GFP^{high} cells in atherosclerotic CX3CR1-GFP mice to be non-monocytes. Further data are required to elucidate the interplay of patrolling monocytes and endothelial cues in atherosclerotic conditions.

In line with a published body of evidence [2–4,35] we posit that the increased endothelial damage in atheroscleortic Nr4a1-knockout mice and the correlation of patrolling intensity with endothelial apoptosis is related to the missing "housekeeping" function of patrolling monocytes. However, the deletion of Nr4a1 has pleiotropic effects, and alternative interpretations of these findings are possible. A hyperinflammatory phenotype of plaque macrophages has been described [19,20], which could affect the microenvironment in a detrimental way. Second, the lack of peripheral patrolling could have indirect effects on plaque patrolling. Third, a local imbalance of monocyte subsets or other leukocytes in situ could adversely affect endothelial fitness of Nr4a1-deficient mice. Future monocyte studies will be greatly improved by using a new enhancer-knockout mouse with specific effects on patrollers but not macrophages [36].

We conclude that large arteries are monitored by patrolling monocytes at steady state, with strong upregulation in hyperlipidemia and atherosclerosis as a potential mechanism to maintain endothelial homeostasis.

AUTHOR CONTRIBUTIONS

A.Q. and K.B. performed most experiments. A.Q., K.B. and S.A. analyzed the data. K.B., D.W., E.E. and M.V. did flow cytometry experiments. A.M. did additonal intravital microscopy experiments. S.A. and Z.M. established and maintained the ILTIS microscopy setup and provided training. J.M. maintained the mouse colony. A.Q. performed electron microscopy. K.B. and K.L. designed the study, and wrote the manuscript.

SOURCES OF FUNDING

This study was funded by R01HL115232 (NHLBI) and NIH HL 115232 to K.L., the Consejo Nacional de Investigaciones Científicas y Técnicas (CONICET) External Fellowship to A.Q. and the Deutsche Forschungsgemeinschaft (DFG) grant BU3247/1 to K.B.

DISCLOSURES

None.

REFERENCES

1. Ley K, Laudanna C, Cybulsky MI, Nourshargh S. Getting to the site of inflammation: the leukocyte adhesion cascade updated. *Nat Rev Immunol*. 2007;7:678–689.
2. Auffray C, Fogg D, Garfa M, Elain G, Join-Lambert O, Kayal S, Sarnacki S, Cumano A, Lauvau G, Geissmann F. Monitoring of blood vessels and tissues by a population of monocytes with patrolling behavior. *Science*. 2007;317:666–670.
3. Carlin LM, Stamatiades EG, Auffray C, Hanna RN, Glover L, Vizcay-Barrena G, Hedrick CC, Cook HT, Diebold S, Geissmann F. Nr4a1-Dependent Ly6Clow Monocytes Monitor Endothelial Cells and Orchestrate Their Disposal. *Cell*. 2013;153:362–375.
4. Hanna RN, Cekic C, Sag D, Tacke R, Thomas GD, Nowyhed H, Herrley E, Rasquinha N, McArdle S, Wu R, Peluso E, Metzger D, Ichinose H, Shaked I, Chodaczek G, Biswas SK, Hedrick CC. Patrolling monocytes control tumor metastasis to the lung. *Science*. 2015;350:985–990.
5. Finsterbusch M, Hall P, Li A, Devi S, Westhorpe CLV, Kitching AR, Hickey MJ. Patrolling monocytes promote intravascular neutrophil activation and glomerular injury in the acutely inflamed glomerulus. *Proc Natl Acad Sci U S A*. 2016;113:E5172-5181.
6. Geissmann F, Manz MG, Jung S, Sieweke MH, Merad M, Ley K. Development of monocytes, macrophages, and dendritic cells. *Science*. 2010;327:656–661.
7. Thomas G, Tacke R, Hedrick CC, Hanna RN. Nonclassical Patrolling Monocyte Function in the Vasculature. *Arterioscler Thromb Vasc Biol*. 2015;35:1306–1316.
8. Imhof BA, Jemelin S, Ballet R, Vesin C, Schapira M, Karaca M, Emre Y. CCN1/CYR61-mediated meticulous patrolling by Ly6Clow monocytes fuels vascular inflammation. *Proc Natl Acad Sci U S A*. 2016;113:E4847-4856.
9. Yona S, Kim K-W, Wolf Y, Mildner A, Varol D, Breker M, Strauss-Ayali D, Viukov S, Guilliams M, Misharin A, Hume DA, Perlman H, Malissen B, Zelzer E, Jung S. Fate mapping reveals origins and dynamics of monocytes and tissue macrophages under homeostasis. *Immunity*. 2013;38:79–91.
10. Hanna RN, Carlin LM, Hubbeling HG, Nackiewicz D, Green AM, Punt JA, Geissmann F, Hedrick CC. The transcription factor NR4A1 (Nur77) controls bone marrow differentiation and the survival of Ly6C- monocytes. *Nat Immunol*. 2011;12:778–785.
11. Woollard KJ, Geissmann F. Monocytes in atherosclerosis: subsets and functions. *Nat Rev Cardiol*. 2010;7:77–86.
12. Hilgendorf I, Swirski FK, Robbins CS. Monocyte fate in atherosclerosis. *Arterioscler Thromb Vasc Biol*. 2015;35:272–279.
13. Robbins CS, Hilgendorf I, Weber GF, Theurl I, Iwamoto Y, Figueiredo J-L, Gorbatov R, Sukhova GK, Gerhardt LMS, Smyth D, Zavitz CCJ, Shikatani EA, Parsons M, van Rooijen N, Lin HY, Husain M, Libby P, Nahrendorf M, Weissleder R, Swirski FK. Local proliferation dominates lesional macrophage accumulation in atherosclerosis. *Nat Med*. 2013;19:1166–1172.
14. Ley K, Miller YI, Hedrick CC. Monocyte and macrophage dynamics during atherogenesis. *Arterioscler Thromb Vasc Biol*. 2011;31:1506–1516.
15. Tacke F, Alvarez D, Kaplan TJ, Jakubzick C, Spanbroek R, Llodra J, Garin A, Liu J, Mack M, van Rooijen N, Lira SA, Habenicht AJ, Randolph GJ. Monocyte subsets differentially employ CCR2, CCR5, and CX3CR1 to accumulate within atherosclerotic plaques. *J Clin Invest*. 2007;117:185–194.
16. Soehnlein O, Drechsler M, Döring Y, Lievens D, Hartwig H, Kemmerich K, Ortega-Gómez A, Mandl M, Vijayan S, Projahn D, Garlichs CD, Koenen RR, Hristov M, Lutgens E, Zernecke A, Weber C. Distinct functions of chemokine receptor axes in the atherogenic mobilization and recruitment of classical monocytes. *EMBO Mol Med*. 2013;5:471–481.
17. Swirski FK, Libby P, Aikawa E, Alcaide P, Luscinskas FW, Weissleder R, Pittet MJ. Ly-6Chi monocytes dominate hypercholesterolemia-associated monocytosis and give rise to macrophages in atheromata. *J Clin Invest*. 2007;117:195–205.
18. Combadière C, Potteaux S, Rodero M, Simon T, Pezard A, Esposito B, Merval R, Proudfoot A, Tedgui A, Mallat Z. Combined inhibition of CCL2, CX3CR1, and CCR5 abrogates Ly6C(hi) and Ly6C(lo)

monocytosis and almost abolishes atherosclerosis in hypercholesterolemic mice. *Circulation*. 2008;117:1649–1657.
19. Hamers AAJ, Vos M, Rassam F, Marinković G, Marincovic G, Kurakula K, van Gorp PJ, de Winther MPJ, Gijbels MJJ, de Waard V, de Vries CJM. Bone marrow-specific deficiency of nuclear receptor Nur77 enhances atherosclerosis. *Circ Res*. 2012;110:428–438.
20. Hanna RN, Shaked I, Hubbeling HG, Punt JA, Wu R, Herrley E, Zaugg C, Pei H, Geissmann F, Ley K, Hedrick CC. NR4A1 (Nur77) deletion polarizes macrophages toward an inflammatory phenotype and increases atherosclerosis. *Circ Res*. 2012;110:416–427.
21. McArdle S, Chodaczek G, Ray N, Ley K. Intravital live cell triggered imaging system reveals monocyte patrolling and macrophage migration in atherosclerotic arteries. *J Biomed Opt*. 2015;20:026005–026005.
22. Jung S, Aliberti J, Graemmel P, Sunshine MJ, Kreutzberg GW, Sher A, Littman DR. Analysis of fractalkine receptor CX(3)CR1 function by targeted deletion and green fluorescent protein reporter gene insertion. *Mol Cell Biol*. 2000;20:4106–4114.
23. Chèvre R, González-Granado JM, Megens RTA, Sreeramkumar V, Silvestre-Roig C, Molina-Sánchez P, Weber C, Soehnlein O, Hidalgo A, Andrés V. High-resolution imaging of intravascular atherogenic inflammation in live mice. *Circ Res*. 2014;114:770–779.
24. Gimbrone MA, García-Cardeña G. Endothelial Cell Dysfunction and the Pathobiology of Atherosclerosis. *Circ Res*. 2016;118:620–636.
25. Davies PF. Hemodynamic shear stress and the endothelium in cardiovascular pathophysiology. *Nat Clin Pract Cardiovasc Med*. 2009;6:16–26.
26. Valignat M-P, Theodoly O, Gucciardi A, Hogg N, Lellouch AC. T lymphocytes orient against the direction of fluid flow during LFA-1-mediated migration. *Biophys J*. 2013;104:322–331.
27. Plump AS, Smith JD, Hayek T, Aalto-Setälä K, Walsh A, Verstuyft JG, Rubin EM, Breslow JL. Severe hypercholesterolemia and atherosclerosis in apolipoprotein E-deficient mice created by homologous recombination in ES cells. *Cell*. 1992;71:343–353.
28. Jongkind JF, Verkerk A, Hoogerbrugge N. Monocytes from patients with combined hypercholesterolemia-hypertriglyceridemia and isolated hypercholesterolemia show an increased adhesion to endothelial cells in vitro: II. Influence of intrinsic and extrinsic factors on monocyte binding. *Metabolism*. 1995;44:374–378.
29. Mata P, Alonso R, Lopez-Farre A, Ordovas JM, Lahoz C, Garces C, Caramelo C, Codoceo R, Blazquez E, Oya M de. Effect of Dietary Fat Saturation on LDL Oxidation and Monocyte Adhesion to Human Endothelial Cells In Vitro. *Arterioscler Thromb Vasc Biol*. 1996;16:1347–1355.
30. Berliner JA, Territo MC, Sevanian A, Ramin S, Kim JA, Bamshad B, Esterson M, Fogelman AM. Minimally modified low density lipoprotein stimulates monocyte endothelial interactions. *J Clin Invest*. 1990;85:1260–1266.
31. Yin Y, Li X, Sha X, Xi H, Li Y-F, Shao Y, Mai J, Virtue A, Lopez-Pastrana J, Meng S, Tilley DG, Monroy MA, Choi ET, Thomas CJ, Jiang X, Wang H, Yang X-F. Early hyperlipidemia promotes endothelial activation via a caspase-1-sirtuin 1 pathway. *Arterioscler Thromb Vasc Biol*. 2015;35:804–816.
32. Salagianni M, Galani IE, Lundberg AM, Davos CH, Varela A, Gavriil A, Lyytikäinen L-P, Lehtimäki T, Sigala F, Folkersen L, Gorgoulis V, Lenglet S, Montecucco F, Mach F, Hedin U, Hansson GK, Monaco C, Andreakos E. Toll-like receptor 7 protects from atherosclerosis by constraining "inflammatory" macrophage activation. *Circulation*. 2012;126:952–962.
33. Nakashima Y, Raines EW, Plump AS, Breslow JL, Ross R. Upregulation of VCAM-1 and ICAM-1 at Atherosclerosis-Prone Sites on the Endothelium in the ApoE-Deficient Mouse. *Arterioscler Thromb Vasc Biol*. 1998;18:842–851.
34. Huo Y, Hafezi-Moghadam A, Ley K. Role of Vascular Cell Adhesion Molecule-1 and Fibronectin Connecting Segment-1 in Monocyte Rolling and Adhesion on Early Atherosclerotic Lesions. *Circ Res*. 2000;87:153–159.
35. Cros J, Cagnard N, Woollard K, Patey N, Zhang S-Y, Senechal B, Puel A, Biswas SK, Moshous D, Picard C, Jais J-P, D'Cruz D, Casanova J-L, Trouillet C, Geissmann F. Human CD14dim monocytes

patrol and sense nucleic acids and viruses via TLR7 and TLR8 receptors. *Immunity*. 2010;33:375–386.
36. Thomas GD, Hanna RN, Vasudevan NT, Hamers AA, Romanoski CE, McArdle S, Ross KD, Blatchley A, Yoakum D, Hamilton BA, Mikulski Z, Jain MK, Glass CK, Hedrick CC. Deleting an Nr4a1 Super-Enhancer Subdomain Ablates Ly6Clow Monocytes while Preserving Macrophage Gene Function. *Immunity*. 2016;45:975–987.

FIGURE LEGENDS

Figure 1: Non-classical monocytes patrol healthy arteries. A) 3D-reconstruction showing a CX3CR1-GFP^{high} monocyte (arrow) patrolling in the lumen of the external carotid artery of a 3-month old CX3CR1$^{+/GFP}$ reporter mouse. The image was aquired in a non-beating artery in situ shortly after an intravital recording. Few tissue-resident CX3CR1-GFP^{high} macrophages are visible in the media/adventitia (right panel, triangle). Scale bar = 50 μm. B) Time-lapse images of a patrolling monocyte (arrow) moving along the endothelium of the carotid artery in a live CX3CR1$^{+/GFP}$ mouse at a heart rate of 380 bpm. Blood flow from right to left. Scale bar = 50 μm. C) Kinetic features of monocytes patrolling healthy arteries. Each dot represents one cell. Mean and S.E.M. shown for 15 patrollers in 5 animals.

Figure 2: Arterial patrolling induced by the TLR7/8 agonist R848. A) Patrollers in the carotid artery imaged before and after topical application of the TLR7/8 agonist R848. The red channel is omitted in the bottom row. Scale bar = 50 μm. Arrows indicate patrolling CX3CR1-GFP^{high} cells. B) Quantification of patrolling CX3CR1-GFP^{high} cells in the carotid artery after R848 stimulation assessed by intravital microscopy. The time course in 3 animals is shown. C) Impact of function blocking anti-LFA-1 and anti-VLA-4 antibodies on patrolling. After 5h R848 treatment, antibodies were injected i.v. and the reduction of numbers was expressed relative to untreated. One-way Anova with Tukey's multiple comparison. *$p<0.05$, **$p<0.01$, n = 3 animals. Mean ± S.E.M shown. D) Tracks are shown as spider plots after aligning the starting positions for untreated, LFA-1, and LFA-1 + VLA-4 inhibited patrollers. Rose plots visualize the overall directionality. Tracks are randomly colored. The arrow indicates the blood flow. E) Patrolling characteristics in R848- and antibody-treated conditions compared to baseline data shown in figure 1. Every dot represents one cell. Data shown as mean ± S.E.M of 3 independent experiments. One-way Anova corrected for multiple comparisons (Tukey) *$p<0.05$, ** $p<0.01$, *** $p < 0.001$.

Figure 3: Hyperlipidemia intensifies monocyte patrolling in arteries. A) The number of patrollers in the carotid artery was determined by intravital microscopy in CX3CR1$^{+/GFP}$ apoE$^{-/-}$ mice on chow diet (6 months old) and CX3CR1$^{+/GFP}$ mice on 4 weeks western diet (WD, 3 months old) compared to baseline as shown in figure 1. Every dot represents one animal. Data as mean ± S.E.M. One-way Anova with Tukey's correction for multiple comparison. B) Representative image of an intravital recording. scale bar = 50 μm. C) Blocking effect of anti-LFA1 and anti-VLA4 antibodies on patrolling. One-way Anova with Tukey's multiple comparison. n=3 animals. **$p<0.01$, *** $p<0.001$. D-F) Analysis of all patrollers in a CX3CR1$^{+/GFP}$ apoE$^{-/-}$ mouse on chow diet in a 45 minute recording shown in B. Patrolling tracks are graphed with absolute (D) or relative coordinates (E). The arrow indicates the direction of the blood flow. The black dot marks the starting position. A rose plot (F) shows the directionality of patrolling (start versus end position). G) Kinetic features compared to baseline condition as shown in figure 1. Data as mean ± S.E.M from 4 (WD) and 6 (apoE$^{-/-}$) animals. Every dot represents one patroller. One-way Anova with Tukey's multiple comparison.

Figure 4: Massive patrolling in arteries with atherosclerotic plaque. A) 3D reconstruction in top down (top) and axial (bottom) view and B) representative frames from an intravital 2D time-lapse sequence of the carotid artery of a CX3CR1$^{+/GFP}$ apoE$^{-/-}$ mouse fed western diet (WD) for 6 weeks. The plasma tracer (red) marks non-plaque regions. Intravascular CX3CR1-GFP^{high} patrollers are marked by arrows. CX3CR1-GFP^{high} macrophages are located in the vessel wall. The 3D image was recorded in a non-beating artery. All scale bars = 50 μm. C) Relative fraction of migration phenotypes of intravascular cells in CX3CR1$^{+/GFP}$ apoE$^{-/-}$ mice fed WD for 6 weeks. 'Patrolling/rolling' indicates alternating patterns during video acquisition. n = 6 animals. Data as mean ± S.E.M. One-way Anova corrected for multiple comparisons (Tukey) * $p<0.05$, ** $p<0.01$. D) Numbers of patrollers observed in intravital microscopy. Every symbol represents one animal. The bar shows data from figure 3 as reference and a dotted line indicates baseline (as shown in figure 1). Unpaired t-test. *** $p < 0.001$. E) Kinetic features of patrollers distant and close to plaque areas.

Data shown as mean ± S.E.M. n = 6 (chow) and 5 (WD) animals per condition. Every symbol represents one cell. Unpaired t-test. *** $p < 0.001$.

Figure 5: Microkinetics and primary monocyte capture in atherosclerosic arteries. A) Velocity profiles of 4 individual cells patrolling in atherosclerotic vessels over time (time resolution 1 frame/s). Cells 1-3 are captured from free flow and show short-term patrolling (< 90s), whereas cell 4 continues patrolling with an intermittent "jump". Green dots indicate capture of a blood-borne cell and red dots detachment. Grayed areas indicate that velocities below 1 µm/s cannot be highly resolved. B) Imaging data of a CX3CR1-GFP^{high} patroller captured from free flow, followed by arrest, patrolling, and a short rolling phase before detachment. Scale bar = 50 µm. See also supplemental movie III-IV.

Figure 6: Correlation of monocyte patrolling and endothelial damage during atherogenesis. A,B) Morphological signs of endothelial cell damage were assessed in control and apoE$^{-/-}$ mice with chow or western diet (WD, 6 weeks) using transmission electron microscopy of carotid arteries. White and black arrows indicate cytoplasmatic edema and vacuolization, respectively. IEL = internal elastic lamina. EC = endothelial cell layer. More images shown in supplemental fig. V. B) Quantification of the extent of the endothelial damage, n = 2/3/2/5 animals (for each condition indicated) with 12-15 sections each. One way Anova with Tukey's multiple comparison. ** $p < 0.01$, *** $p < 0.001$. c) Linear regression of endothelial cell damage as shown in (b) and active patrolling monocytes (per field of view) observed in situ by intravital microscopy. Pearson correlation, R^2 and p-value indicated.

Figure 7: Enhanced endothelial damage in atherosclerotic arteries of patroller-deficient Nr4a1$^{-/-}$ mice. A,B) Explanted aortas of apoE$^{-/-}$ Nr4a1-knockout or control mice fed 6 weeks western diet were flushed, and the flow-through was analyzed by flow cytometry. n = 3 per group. Unpaired t-test. * $p < 0.05$, ** $p < 0.01$ c) Transmission electron micrographs of apoE$^{-/-}$ Nr4a1$^{-/-}$ carotid arteries. Nuclear condensation (left panel) and chromatin fragmentation (right panel) are depicted as signs of severe cell damage. More images shown in supplemental fig. V. d) Quantification of the severity of endothelial cell death (number of lesions per section as defined in the method section). n = 3 animals with 12-15 sections each. Data shown as mean +/- S.E.M. Unpaired t-test. *** $p < 0.001$. **Table 1:** Using ILTIS microscopy, monocyte patrolling in CX3CR1$^{+/GFP}$ mice was analyzed in both the ear microcirculation and the carotid artery, and motion characteristics were determined. Data shown as mean ± S.D. n=5/15 (carotid) and 2/9 (ear) animals/cells. Data by Auffray et al. [2] was added as independent reference.

NOVELTY AND SIGNIFICANCE

What Is Known?

- The endothelium of microcirculatory vessels is patrolled by intraluminal non-classical monocytes.
- Endothelial damage triggers accumulation of patrolling monocytes to initiate scavenging and repair processes.

What New Information Does This Article Contribute?

- Non classical monocytes patrol large arteries with different migratory and molecular properties compared to the microcirculation.
- Patrolling monocytes accumulate in hyperlipidemia and atherosclerosis, and their depletion aggravates endothelial damage.
- Therapeutic modulation of patrolling activity could be a novel way to reduce atherosclerosis.

Patrolling monocytes are crucial for the endothelial integrity of microcirculatory vessels. Their relevance in large atherosclerotic arteries had not been investigated. Here, we establish that carotid arteries are actively surveyed by non classical monocytes in healthy mice, suggesting that patrolling is an intraluminal surveillance mechanism throughout the entire vascular system. Arterial patrolling is markedly upregulated after TLR7 stimulation (viral danger signals), in hyperlipidemia and in atherosclerotic conditions. Monocyte migratory and molecular properties are different compared to the microcirculation, e.g. in terms of adhesion and chemokine receptor requirements. The number of active patrolling monocytes correlates with the severity of endothelial damage during atherogenesis. Mice deficient in non classical monocytes show aggravated endothelial damage in atherosclerotic arteries. Together, these data establish the concept of arterial monocyte patrolling, define the migratory and molecular phenotype of patrolling monocytes, and suggest they have an endothelial-protective role.

Table 1

		carotid artery	ear microcirculation	ear microcirculation[2]
microscopy technique		ILTIS	ILTIS (10-stack in Z)	confocal (10-stack in Z)
duration	min	4.7 ± 3.1	14 ± 3	range 9-12
length	µm	134 ± 58	249 ± 83	~220
displacement	µm	31 ± 18	162 ± 20	~100
confinement ratio		0.22 ± 0.13	0.63 ± 0.13	~0.5
velocity	µm/min	36 ± 12	17 ± 5	12

Table 2: Synopsis of all parameters aquired by ILTIS. All data were obtained in 17 min long videos with a field of view (FOV) of 455 x 227 µm. Data shown as mean ± standard deviation. R848 = 5h topical application at 1 mg/ml. Western diet (WD) = C57Bl/6J mice on 4 weeks western diet. apoE$^{-/-}$ = 4-6 month old mice on chow diet. apoE$^{-/-}$ +WD = fed WD for 6 weeks. Plaque-distant and –close patrollers were separately analyzed.

	unit	basal	R848	WD	apoE$^{-/-}$	apoE$^{-/-}$ +WD	
						distant	close
patroller	#/FOV	3 ± 2	29 ± 18	34 ± 11	29 ± 19	80 ± 12	
	fold	1	7.9 ± 4.9	9.2 ± 3.2	8.1 ± 5.2	22.1 ± 3.5	
velocity	µm/s	0.60 ±	0.33 ±	0.50 ±	0.58 ±	0.53 ±	0.34 ±
	µm/min	36 ± 12	19 ± 6	30 ± 7	34 ± 14	32 ± 7	20 ± 6
duration	s	284 ± 190	343 ± 309	364 ± 236	437 ± 330	224 ± 204	463 ± 365
length	µm	134 ± 58	124 ± 116	140 ± 79	263 ± 287	137 ± 78	167 ± 22
confineme		0.22 ±	0.10 ±	0.23 ±	0.27 ±	0.20 ±	0.05 ±
displaceme	µm	31 ± 18	12 ± 22	30 ± 20	68 ± 79	20 ± 18	15 ± 17
		n=15	n=64	n=23	n=44	n=55	n=29

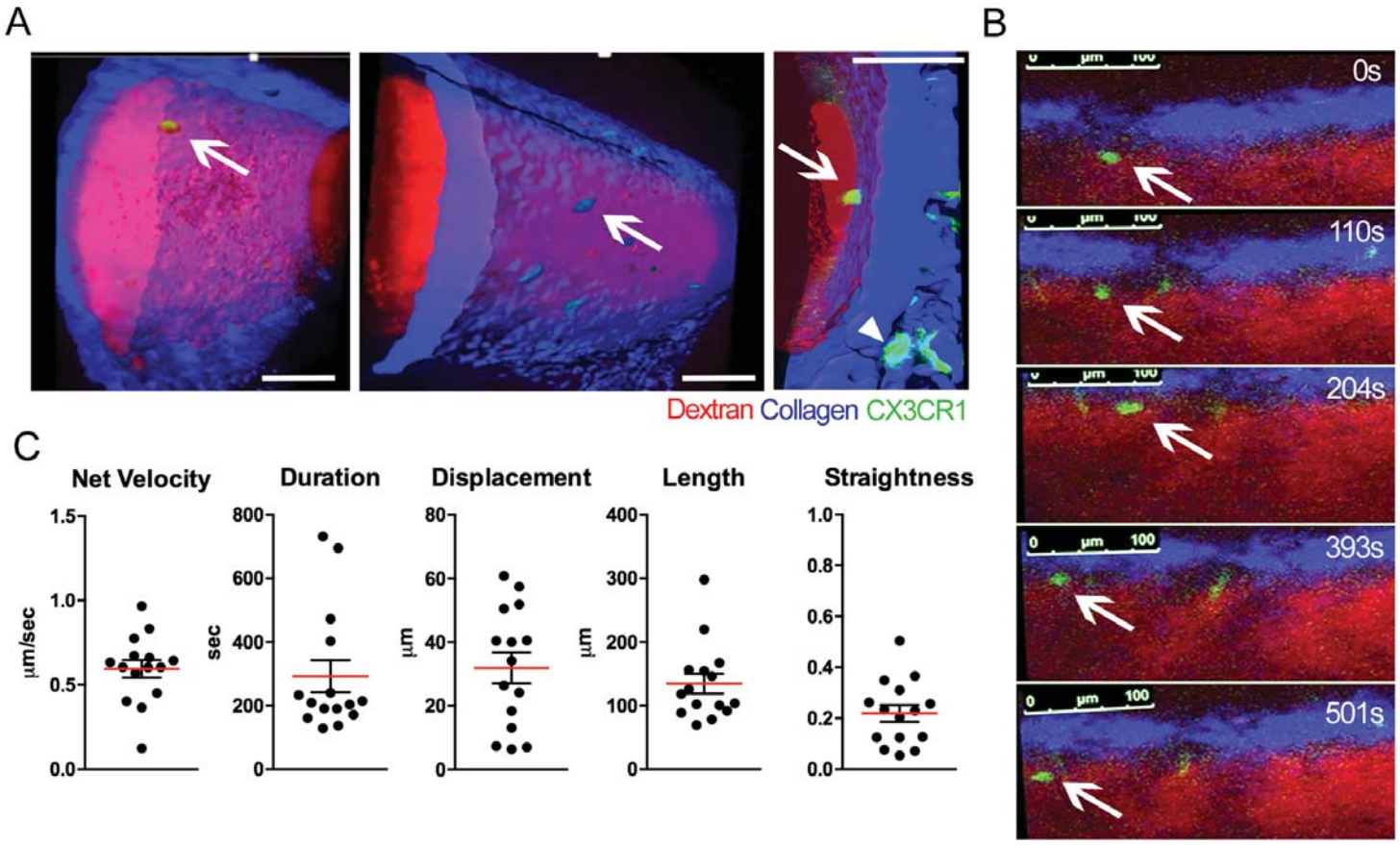

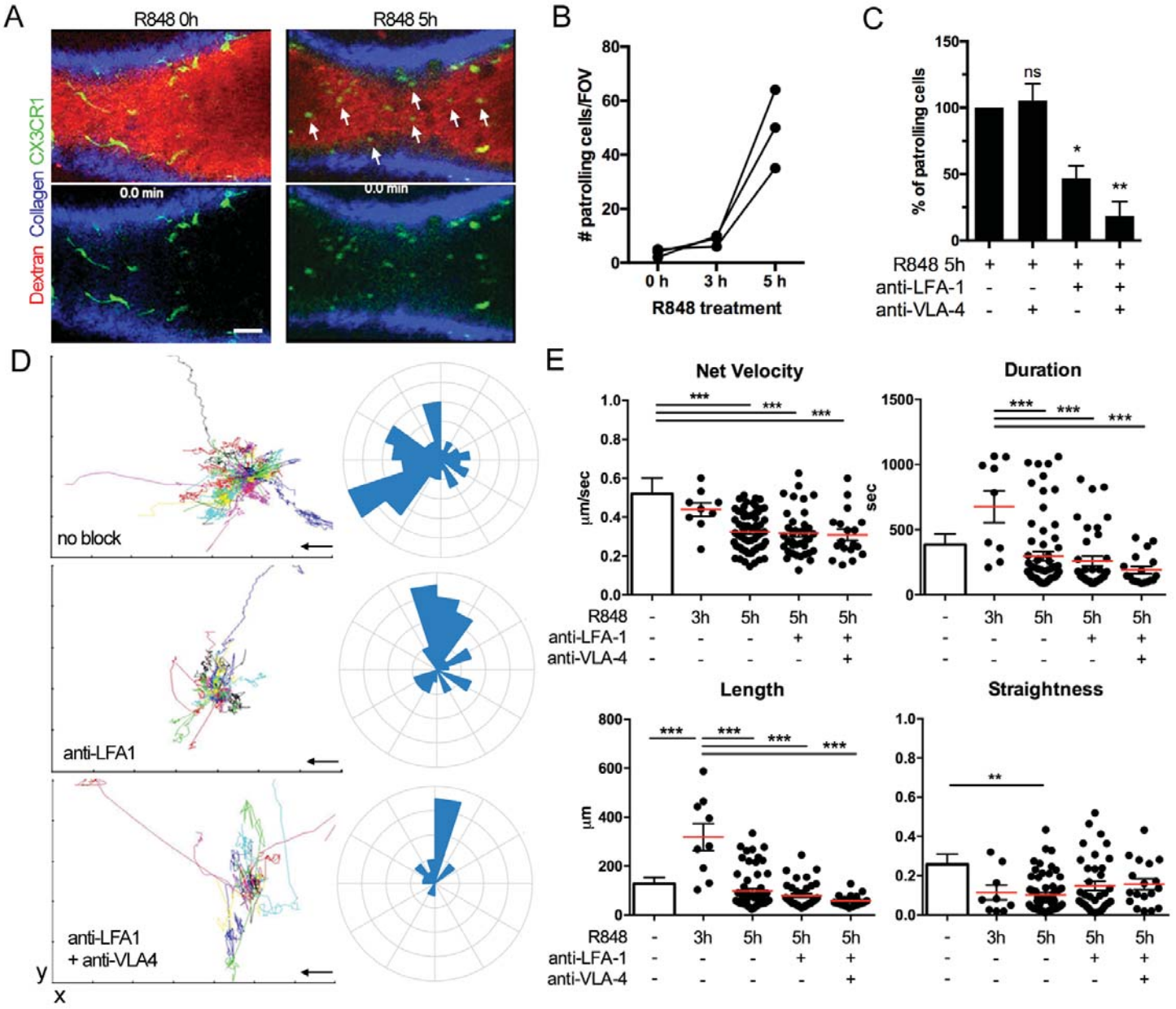

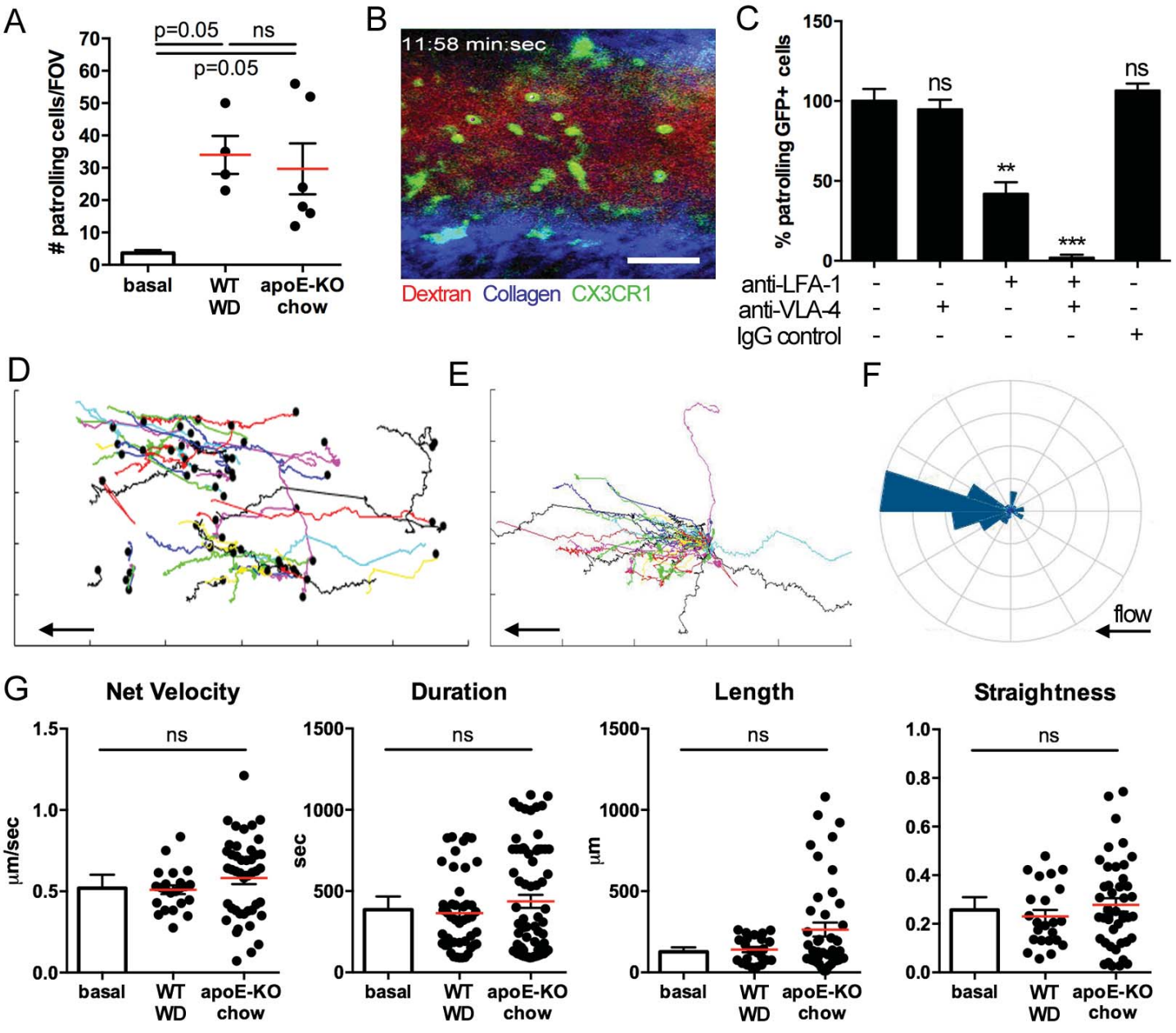

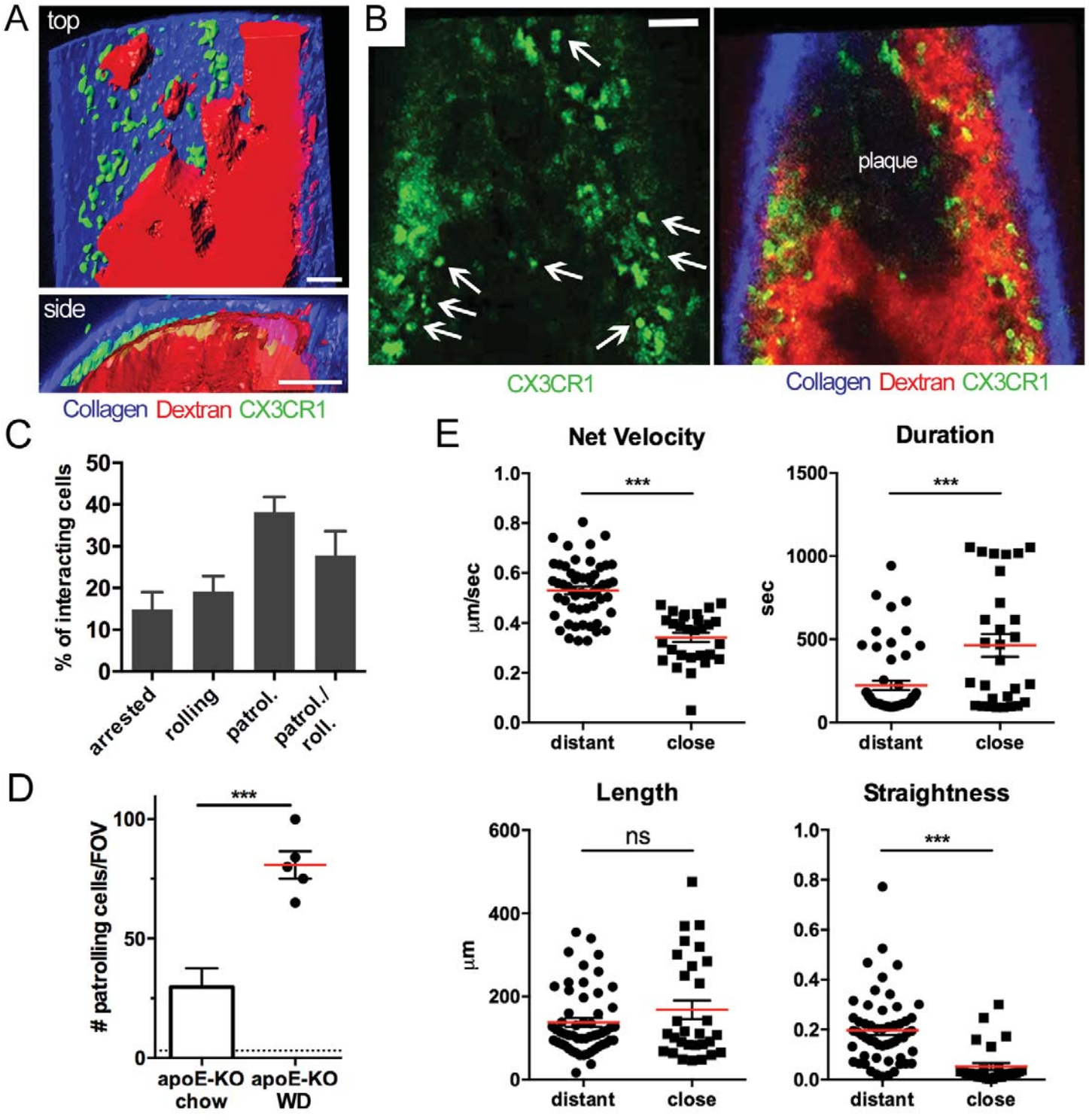

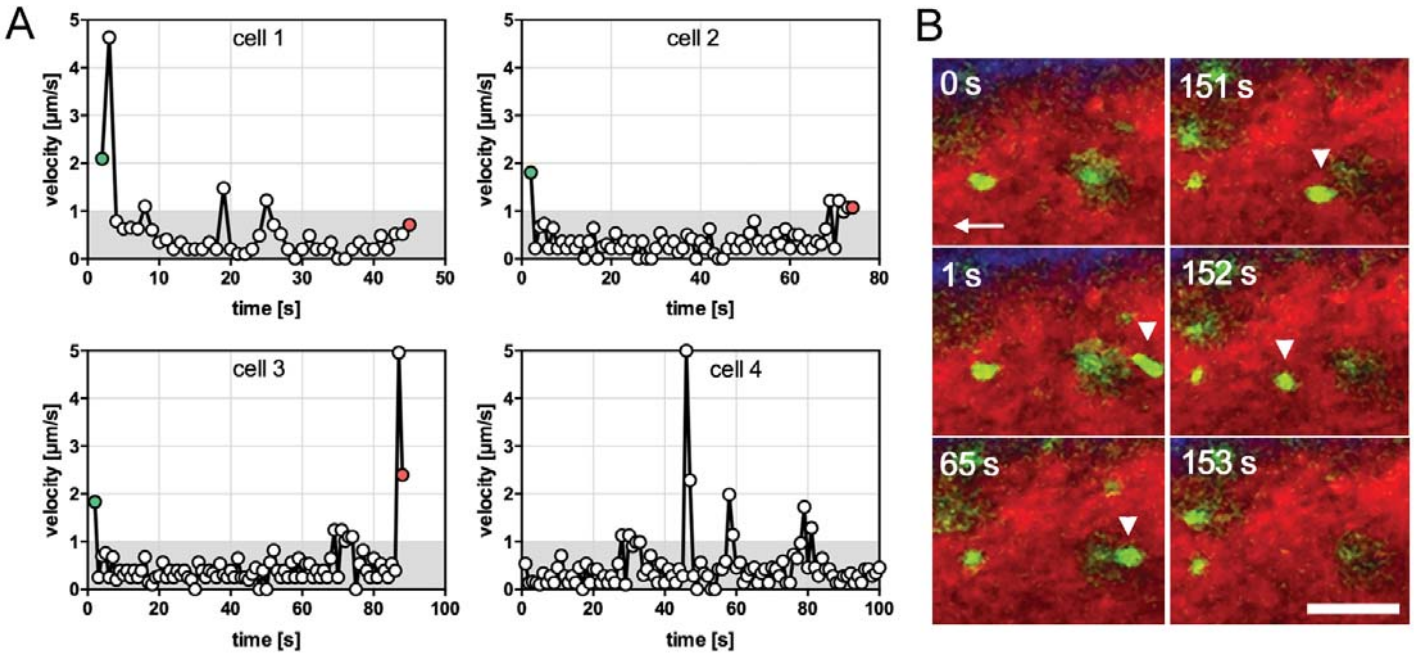

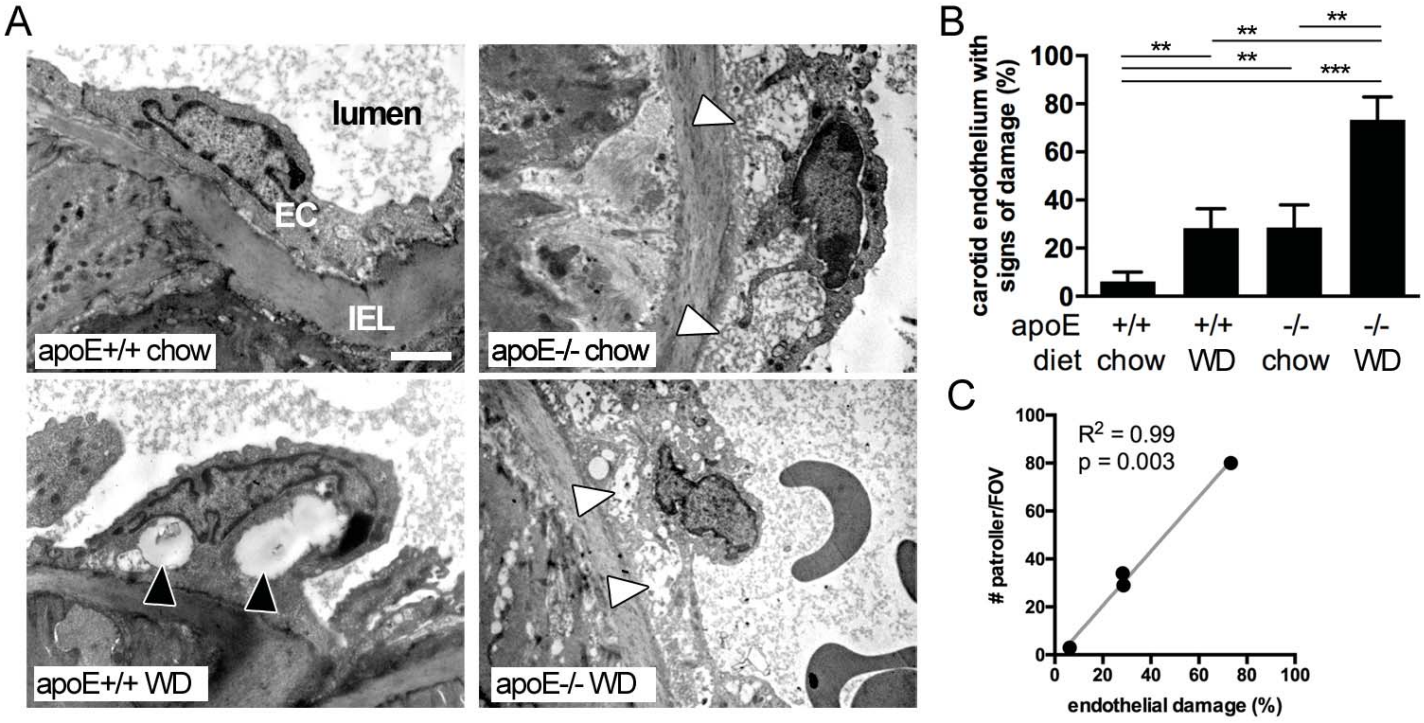

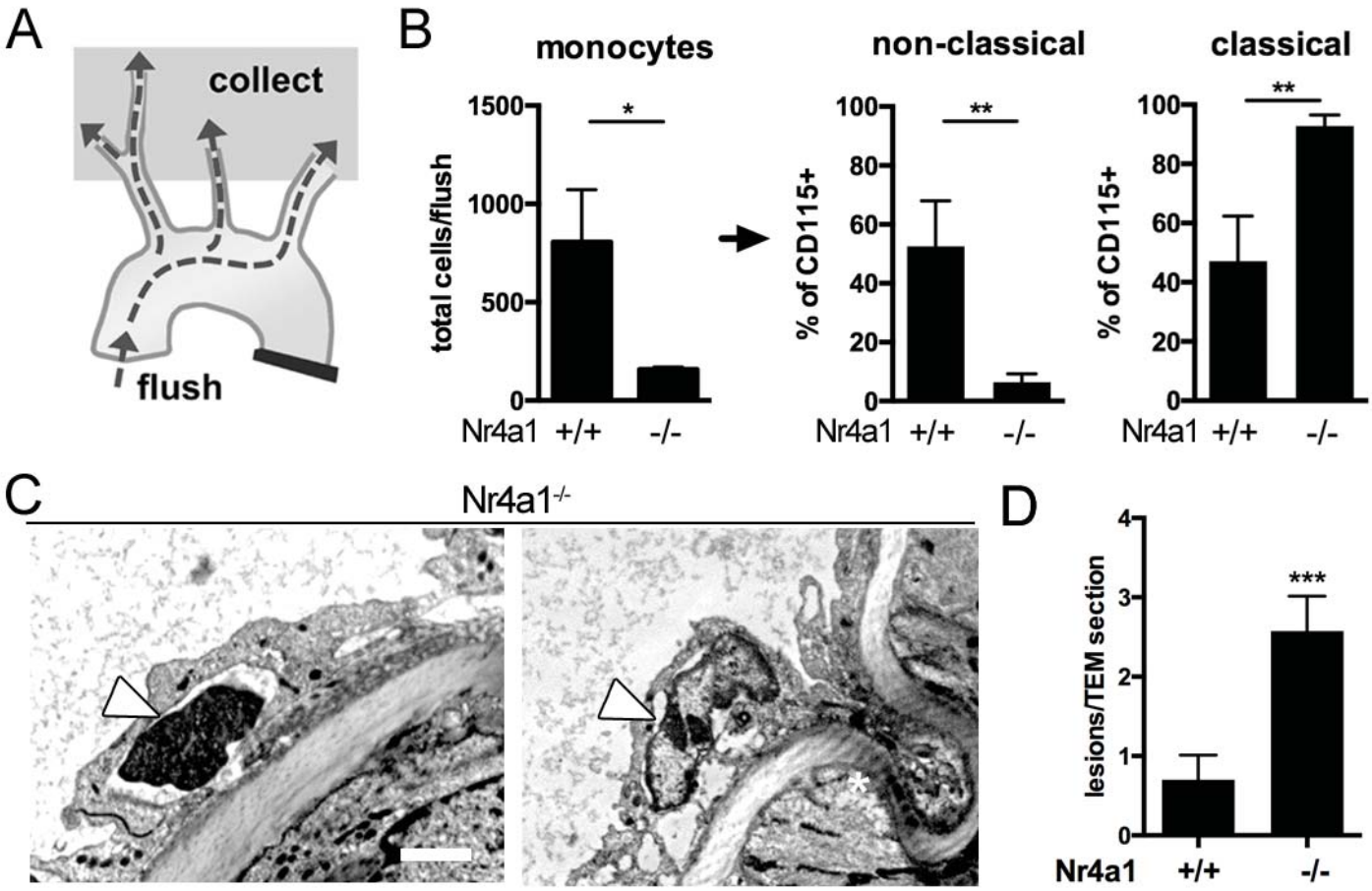

Circulation Research
JOURNAL OF THE AMERICAN HEART ASSOCIATION

Endothelial Protective Monocyte Patrolling in Large Arteries Intensified by Western Diet and Atherosclerosis

Amado Quintar, Sara McArdle, Dennis Wolf, Alex Marki, Erik Ehinger, Melanie Vassallo, Jacqueline F Miller, Zbigniew Mikulski, Klaus Ley and Konrad Buscher

Circ Res. published online March 16, 2017;
Circulation Research is published by the American Heart Association, 7272 Greenville Avenue, Dallas, TX 75231

Print ISSN: 0009-7330. Online ISSN: 1524-4571

SUPPLEMENTAL MATERIAL
Quintar A et al.

Detailed Methods

Materials
Blocking rat anti-mouse antibodies to VLA-4 (clone PS/2) and LFA-1 (clone TIB 217) free of azide and endotoxin were purified from hybridomas (ATCC). Dextran-Texas Red (70,000 MW) was purchased from Thermo Fisher Scientific. The R848 reagent was purchased from Invivogen and stored at -20°C as 1 mg/ml stock solution.

Animals
CX3CR1-GFP reporter mice were provided by S. Jung (Weizmann Institute, Israel) and back-crossed onto C57BL/6J until a genetic purity of > 99% was achieved (SNP analysis by Dartmouse, Dartmouth College, USA). ApoE$^{-/-}$ mice were obtained from Jackson Laboratory (stock number: 002052). CX3CR1-GFP and apoE$^{-/-}$ mice were crossed, resulting in CX3CR1$^{+/GFP}$ apoE$^{-/-}$ mice [1]. Homogenous expression of CX3CR1-GFP leads to a functional protein knockout [2]. In experiments comparing CX3CR1$^{+/GFP}$ and CX3CR1$^{GFP/GFP}$ littermates were used. Nr4a1-deficient mice on apoE$^{-/-}$ background were used as previously described [3]. All animal experiments were approved by the local animal ethics committee. Mice were kept under specific pathogen-free conditions in an AAALAC-approved barrier facility with food and water ad libitum and on a 12h day/night cycle. At 6 weeks of age, mice were placed on a western diet (42% fat, Envigo). The CX3CR1 wildtype allele was screened using the following primers: 5′ -TTC ACG TTC GGT CTG GTG GG-3 and 5′ -CGT CTG GAT GAT TCG GAA GTA GC-3. The GFP knock-in construct was screened with the following primers: 5′ -TAA ACG GCC ACA AGT TCA GCG-3′ and 5′ -TAC TCC AGC TTG TGC CCC AGG ATG TT-3.

Intravital live cell triggered imaging system (ILTIS)
Technical details of the ILTIS setup have been described before [1]. Mice were anesthetized by i.p. ketamine/xylazine (100/10 mg/kg) injection and the fur around the neck and the thighs was removed with lotion. Preparation of the large arteries was done carefully with minimal handling to prevent surgery-related inflammation. The adventitia was not removed. Tissue was kept moist with phophate-buffered saline at 35-37°C. In some experiments a jugular catheter at the contralateral side was inserted for antibody injections or blood draws. The trachea was intubated using PE90 tubing. The animal was kept on a temperature controlled heating pad with a rectal sonde (feedback loop) throughout the experiment at 37°C. A pulse oxymeter was installed at the right tigh. Supplemental oxygen was given to keep the peripheral oxygen saturation at > 95%. Texas red-dextran as blood tracer (5 mg/ml in 100 µl) was injected i.v. prior to imaging. Supplemental anesthetic was applied at 30-60 min intervals. All imaging experiments were conducted on a Leica SP5 system with a water-dipping objective (Olympus XLUMPLFL 20X NA 0.95) and an objective heater. The system is composed of a DM6000 microscope, a Ti-Sapphire laser (Chameleon Ultra II, Coherent), tuned to 920 nm for all experiments, a resonant scanhead for fast scanning, and a Leica trigger box. Three NDD detectors were used in most of the experiments: 460/40 for second harmonics, 513/50 for GFP, and 640/40 for detecting texas red. Videos were recorded in 512 x 256 pixel resolution for 30 – 90 minutes. Using these instrument settings, we did not

observe autofluorescent structures in the vessel wall. Distorted vessel borders (e.g. hourglass shape) can occur when the artery is slightly bent at the focal plane. No photo-toxic effects were obvious in longer recordings. The number of patrollers per field of view was corrected for plaque regions. Under ketamine/xylazine anesthesia, the heart rate was typically at about 300 – 400 bpm. An Arduino-based circuit allowed image acquisition in triplets triggered by signal of the pulse oxymeter [1]. For integrin blocking experiments, videos were aquired before and after injection. After 15-20 min video acquisition, 50 µl of anti-LFA-1 (1.04 mg/ml) was injected through the jugular catheter. After recording for 15-20 min, 50 µl of anti-VLA-4 (0.84 mg/ml) was injected in the same way for sequential blocking.

Noise filtering

After ILTIS post-processing, which included frame selection and 2D registration [1,4] using the Fiji software [5], the remaining noise was filtered. The centroid position of each cell was found in Imaris, which outputs a position calculated to more precision than the resolution of the image (0.89 µm per pixel). This led to slow or stopped cells showing sub-pixel back-and-forth motion. In some cases, this greatly contributed to the total distance the cell traveled or its velocity. A custom Matlab script was written to remove this spurious effect and discard any sub-pixel motion. The change in position of each cell between frames was calculated and any movement less than 1 pixel was discarded (x and y motion were considered separately). The cell was then repositioned to its starting position and the next timepoint was analyzed. This process improved the accuracy of the tracks without changing the total displacement of the cells.

Cell tracking and data analysis

After post-processing, a final frame rate of 1 – 1.5 frames/s was achieved. In all movies analyzed, patrolling GFP+ cells were detected using an absolute intensity threshold and tracked using Imaris' autoregressive motion algorithm. The coordinates were exported to Matlab for further analysis. Any gaps in the coordinates due to out-of-focus frames were filled in using linear interpolation. The exact direction of blood flow in each movie was estimated by the angle of the collagen (SHG signal) in the arterial wall. To reduce the effect of noise on calculations, any change in measured position smaller than 1 pixel (890 nm) was removed (adjusting x and y positions separately). Only cell tracks lasting longer than 90 sec were considered patrolling. This threshold allowed to minimize false positive patrollers in videos with residual artifact movement after post-processing. For quantification, patrolling monocytes were tracked over 17 min in each movie unless indicated otherwise. Since in some movies not the entire surface of the endothelium could be visualized (tilted vessel), calculations were normalized by the imaged surface area of the artery. Fast cells moving at over 100 µm/min were considered as rolling cells. The confinement ratio was calculated by the distance traveled (start vs. end position) divided by the track length whereby 1 = straight track. In vessels with atherosclerotic plaques (determined by the lack of plasma tracer), the number of patrolling monocytes was corrected for the visible endothelial area. Areas close and distant to the plaque were defined based on the lack of plasma tracer (which indicates a plaque region). GFP+ cells adjacent to this region (within about 2 cell diameters) were counted as "close", whereas all other cells were counted as "distant". Frame by frame cell tracking was done using the manual cell tracking plugin in Fiji.

Arterial flushing

Animals were euthanized and as much blood as possible was removed via cardiac puncture. After exposure of the aortic arch, the proximal thoracic aorta was ligated. The left ventricular

outflow tract was cannulated using PE50 tubing. The aorta including its large branches (up to the common carotid arteries) were removed and dipped in PBS to remove extravasal debris and erythrocytes. Then, the vessels were flushed with 5 ml PBS (room temperature) by applying a constant pressure over 2 min, and the flow-through was collected on ice. Flow cytometry showed a viability of > 95%.

TUNEL apoptosis assay

The TUNEL fluorescein apoptosis assay by Roche (In situ cell death detection kit, fluorescein) was used to determine apoptotic endothelial cells in the aorta. $Nr4a1^{-/-}$ or $Nr4a1^{+/+}$ on $apoE^{-/-}$ background (age 6 month on chow diet) were used. Mice were anaesthetized with isofluorane and 5 μg of a CD31-AF647 antibody was injected i.v.. After 5 min, the mouse was euthanized, and the aorta (arch, main bifurcations, thoracic aorta) harvested. The kit was employed according to the manufacture's instructions. A negative control did not include the terminal transferase (labeling solution only). A positive control included a DNAse I treated section of the aorta (a distal part of the specimen was separated). After labeling, all specimen were mounted on a cover slide with the endothelial side up. Images were taken using a Leica SP8 confocal microscope with a 25x water immersion objective using the tiles function (4 adjacent field of views). In the image analysis, only CD31+ TUNEL+ events were counted that also featured the shape and size of endothelial cells (as compared to the positive control).

Transmission electron microscopy

Mice were fixed by i.a. perfusion with 4% formaldehyde. Carotid arteries were then fixed in Karnovsky fixative containing 1.5% (v/v) glutaraldehyde and 4% (w/v) formaldehyde in 0.1M cacodylate buffer overnight, treated with 1% osmium tetroxide for 2 h, dehydrated, and embedded in Araldite. For ultrastructural studies, thin sections were cut with a diamond knife on Porter-Blum MT2 and JEOL JUM-7 ultramicrotomes and imaged using a Zeiss LEO 906E electron microscope. One carotid section was taken every 70 μm (a total of 12 sections per tissue block) and examined at 4800x and 6000x magnification. The morphological analysis of endothelial cell damage was performed as previously described [6,7]. Ultrastructural signs of endothelial lesions include loss of electrodensity, small, medium, and big cytoplasmic vacuoles (incipient signs), cytoplasmic edema, chromatin fragmentation, nuclear condensation, exnucleation, cell shedding and denudation (signs of severe damage). The extent of endothelial damage (figure 6) was calculated by measuring the affected area (including incipient and severe lesions) and referred as a percentage of the total endothelial area per cross section in each sample using ImageJ. For figure 7, severe cell death-associated endothelial lesions were quantified and expressed as number of lesions per cross section of the carotid artery.

Statistics

The number of patrolling cells and their kinetics are represented as mean ± S.E.M. Statistical tests are indicated in the figure legends. All statistical analysis was performed with the Prism GraphPad Software.

References

1. McArdle S, Chodaczek G, Ray N, Ley K. Intravital live cell triggered imaging system reveals monocyte patrolling and macrophage migration in atherosclerotic arteries. *J Biomed Opt*. 2015;20:026005–026005.
2. Jung S, Aliberti J, Graemmel P, Sunshine MJ, Kreutzberg GW, Sher A, Littman DR. Analysis of fractalkine receptor CX(3)CR1 function by targeted deletion and green fluorescent protein reporter gene insertion. *Mol Cell Biol*. 2000;20:4106–4114.
3. Hanna RN, Shaked I, Hubbeling HG, Punt JA, Wu R, Herrley E, Zaugg C, Pei H, Geissmann F, Ley K, Hedrick CC. NR4A1 (Nur77) deletion polarizes macrophages toward an inflammatory phenotype and increases atherosclerosis. *Circ Res*. 2012;110:416–427.
4. Ray N, McArdle S, Lay K, Acton S. MISTICA: Minimum Spanning Tree-based Coarse Image Alignment for Microscopy Image Sequences. *IEEE J Biomed Health Inform*. 2015;
5. Schindelin J, Arganda-Carreras I, Frise E, Kaynig V, Longair M, Pietzsch T, Preibisch S, Rueden C, Saalfeld S, Schmid B, Tinevez J-Y, White DJ, Hartenstein V, Eliceiri K, Tomancak P, Cardona A. Fiji: an open-source platform for biological-image analysis. *Nat Methods*. 2012;9:676–682.
6. True AL, Olive M, Boehm M, San H, Westrick RJ, Raghavachari N, Xu X, Lynn EG, Sack MN, Munson PJ, Gladwin MT, Nabel EG. Heme oxygenase-1 deficiency accelerates formation of arterial thrombosis through oxidative damage to the endothelium, which is rescued by inhaled carbon monoxide. *Circ Res*. 2007;101:893–901.
7. Sugiyama T, Kawamura K, Nanjo H, Sageshima M, Masuda H. Loss of arterial dilation in the reendothelialized area of the flow-loaded rat common carotid artery. *Arterioscler Thromb Vasc Biol*. 1997;17:3083–3091.

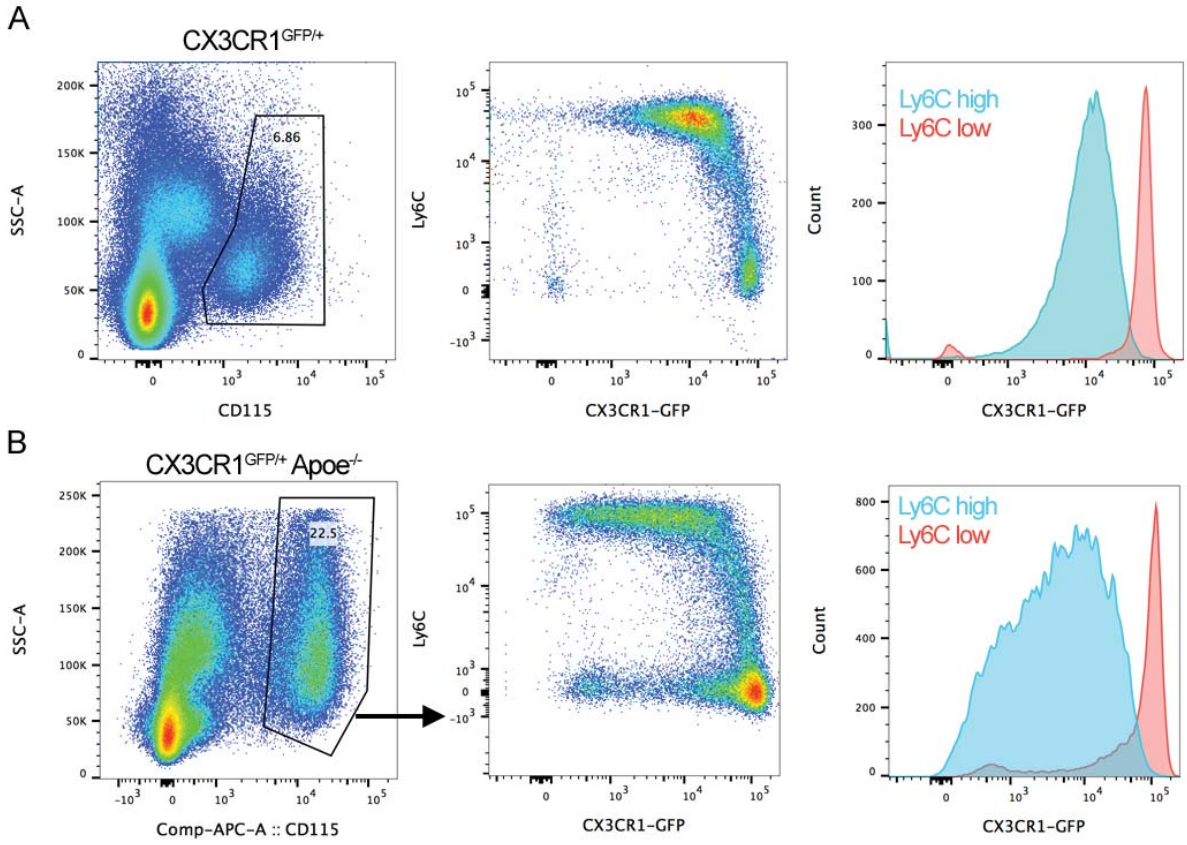

Supplemental figure I: Representative flow cytometry data of the CX3CR1-GFP expression in live single CD115+ monocytes in CX3CR1$^{+/GFP}$ mice (top) on chow diet and CX3CR1$^{+/GFP}$ apoE$^{-/-}$ on high fat diet (6 weeks) mice (bottom). Non-classical monocytes are Ly6C^{low} and GFP^{high} and classical monocytes are Ly6C^{high} and GFP^{medium}.

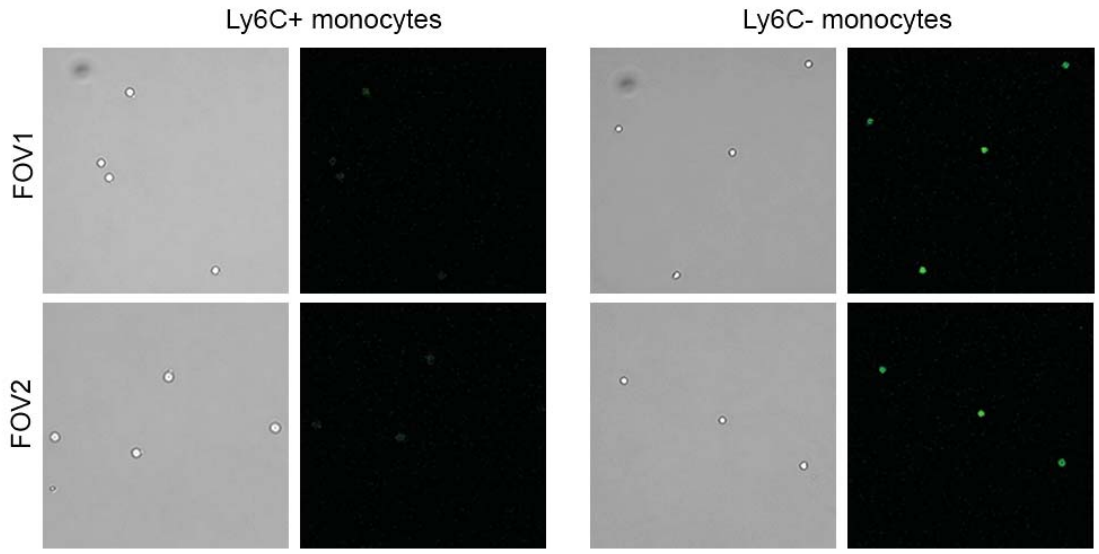

Supplemental figure II: Ly6C^{high} and Ly6C^{low} monocyte populations were sorted from blood of CX3CR1$^{+/GFP}$ mice and imaged using ILTIS. Two field of views (FOV) with brightfield and GFP channel are shown. Only the GFP signal of Ly6G^{low} monocytes is clearly detectable.

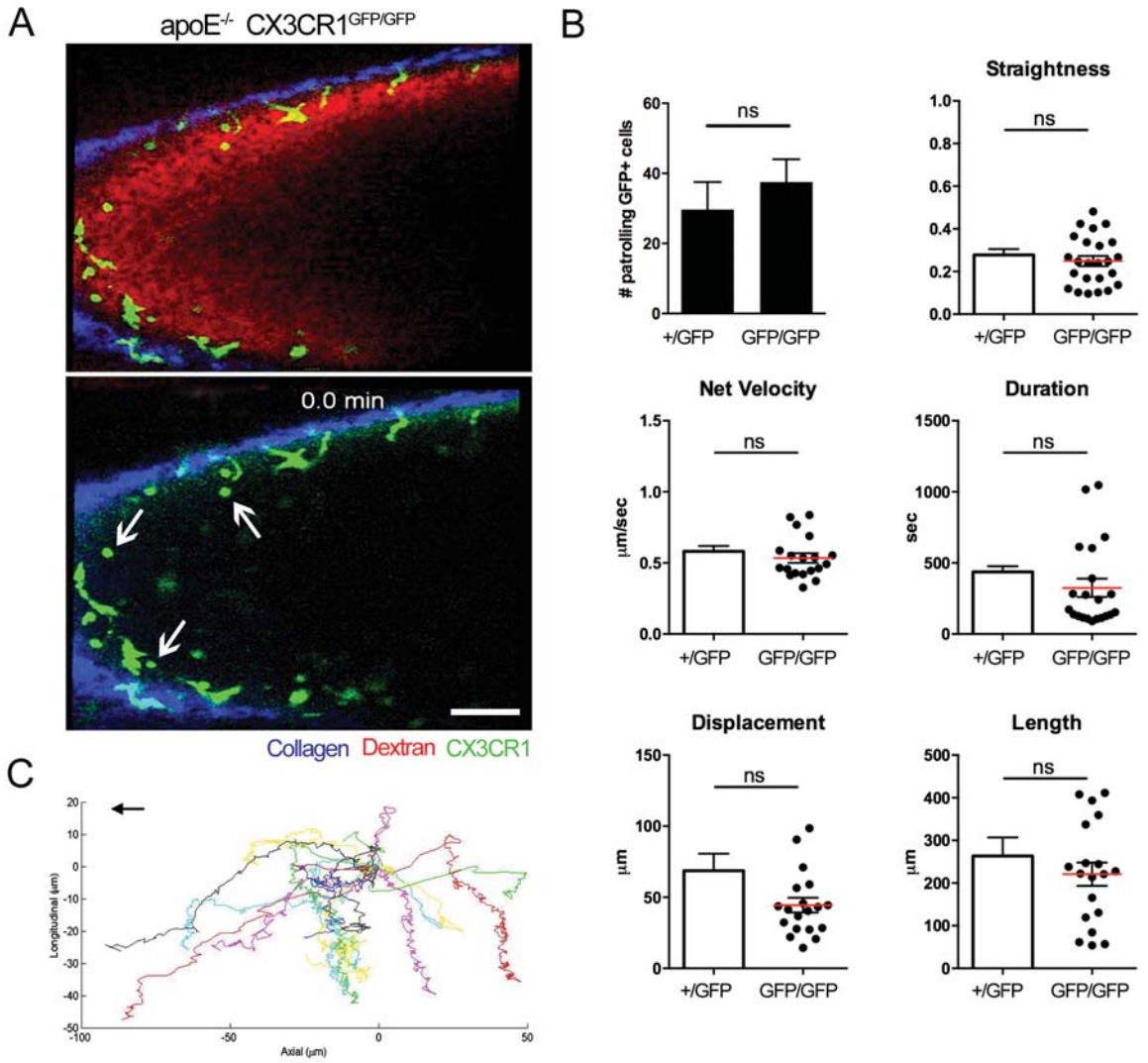

Supplemental figure III: Arterial monocyte patrolling is independent of CX3CR1. A) Image from a time-lapse sequence of the external carotid from a 5-month-old homozygous CX3CR1$^{GFP/GFP}$ apoE$^{-/-}$ mouse fed chow diet showing numerous CX3CR1-GFP monocytes with patrolling activity (arrows). Bar represents 50 µm. B) Average number of patrolling monocytes and motion characteristics are shown compared to heterozygous CX3CR1$^{+/GFP}$ apoE$^{-/-}$ mice (as in figure 1). Every dot represents one patroller. Data shown as mean ± S.E.M. Unpaired t test. C). Monocyte tracks in one video acquisition in a CX3CR1$^{GFP/GFP}$ mouse over 17 min. Tracks are aligned to their starting position and are randomly colored. The arrow indicates the blood flow.

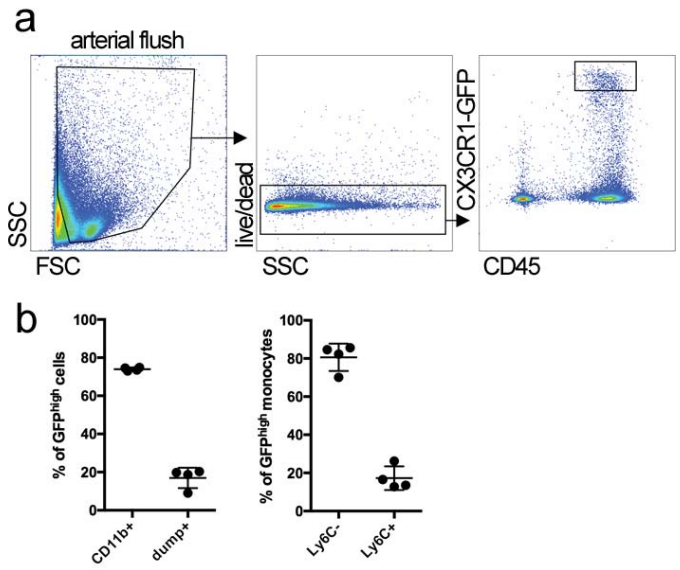

Supplemental figure IV: Aorta explants of CX3CR1$^{+/GFP}$ apoE$^{-/-}$ mice fed 6 weeks western diet were flushed and the flow through (= intraluminal cells) was analyzed by flow cytometry. a) Gating strategy on all live CD45+ GFP^{high} cells. b) Percentage of CD11b+ monocytes, their Ly6C-high and low subsets (right panel), and dump channel (CD3, CD19, Ly6G, NKp46) positive cells. Every dot represents one aorta. n = 4. About 80% of GFP^{high} cells are monocytes, of which about 80% are patrolling monocytes.

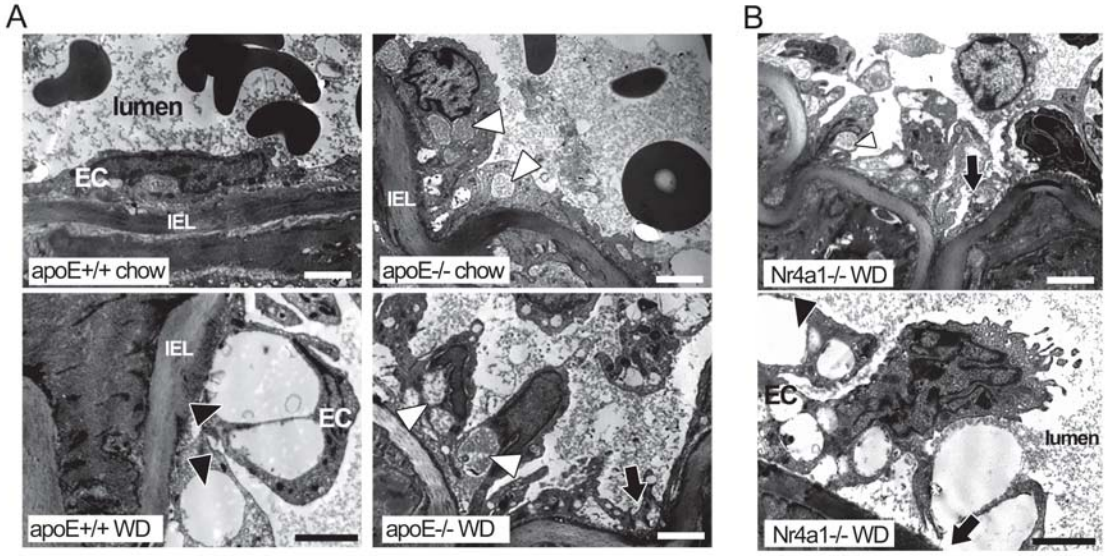

Supplemental figure V: Ultrastructural evidence of endothelial damage in the carotid artery during atherogenesis. Quantification shown in figure 6 and 7. EC: endothelial cell; IEL: internal elastic layer. Scale bar = 5 µm. A) apoE$^{+/+}$ and apoE$^{-/-}$ mice with chow or western diet (WD, 4-6 weeks). Incipient lesions include small to medium sized cytoplasmic vacuoles (white arrowheads). Big vacuoles (black arrowheads) displace the nucleus. B) apoE$^{-/-}$ Nr4a1$^{-/-}$ mice on western diet exhibit more severe endothelial lesions compared to apoE$^{-/-}$ Nr4a1$^{+/+}$ controls. Endothelial shedding and denudation indicated by black arrows.

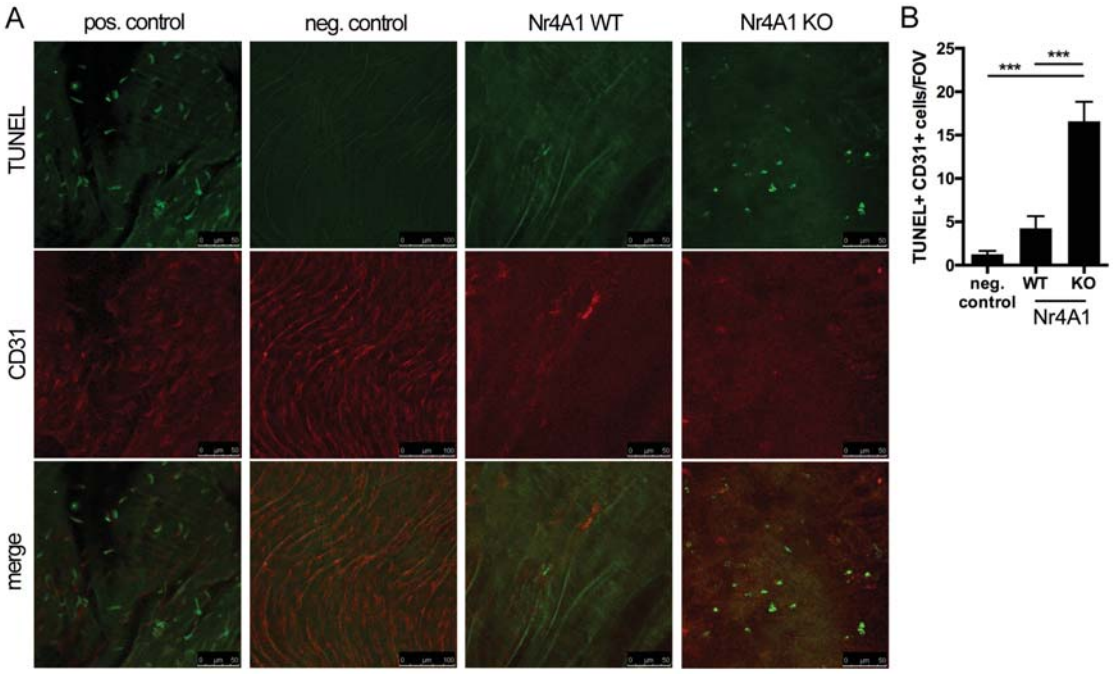

Supplemental figure VI: TUNEL fluorescein apoptosis assay in endothelial cells of the aortic arch in Nr4a1$^{-/-}$ apoE$^{-/-}$ mice compared to Nr4a1$^{+/+}$ apoE$^{-/-}$ controls. A) CD31 (PECAM-1) was used to identify the endothelial cell layer, and a DNAse-I treated sample served as a positive control. Representative images for each condition are shown. B) Quantification of TUNEL+ CD31+ endothelial cells per field of view (FOV). Data shown as mean +/- S.E.M. n = 8 (neg. control), 8 (WT) and 12 (KO) FOVs of 2 animals each. One-way ANOVA with Tukey's correction for multiple comparison. *** $p < 0.001$.

Movie legends

Movie I: 3D ILTIS microscopy showing monocyte patrolling in the carotid artery of CX3CR1$^{+/GFP}$ mice fed high-fat diet for 4 weeks. Vessel wall macrophages are also GFP positive but are sessile. Blue = collagen; green = CX3CR1-GFP. Scale bar 70 μm.

Movie II: Monocyte interaction (patrolling, rolling, arrest) in the carotid artery of a 4 month old CX3CR1$^{+/GFP}$ apoE$^{-/-}$ mice on chow diet as imaged by 2D ILTIS microscopy. Areas of dim/missing red signal indicate plaque regions. Blue = collagen; green = CX3CR1-GFP; red = luminal dextran. Scale bar 50 μm.

Movie III: Example of monocyte patrolling in the carotid artery of a CX3CR1$^{+/GFP}$ apoE$^{-/-}$ mice on high fat diet for 6 weeks. Scale bar = 25 μm.

Movie IV: Example of monocyte patrolling in the carotid artery of a CX3CR1$^{+/GFP}$ apoE$^{-/-}$ mice on high fat diet for 6 weeks. Scale bar = 25 μm.